



HAL
open science

2D numerical contributions for the study of non-cohesive sediment transport beneath tidal bores

Yoga Satria Putra, Anthony Beaudoin, Germain Rousseaux, Lionel Thomas,
Serge Huberson

► **To cite this version:**

Yoga Satria Putra, Anthony Beaudoin, Germain Rousseaux, Lionel Thomas, Serge Huberson. 2D numerical contributions for the study of non-cohesive sediment transport beneath tidal bores. *Comptes Rendus Mécanique*, 2019, 347 (2), pp.166-180. 10.1016/j.crme.2018.11.004 . hal-02282788

HAL Id: hal-02282788

<https://hal.science/hal-02282788>

Submitted on 21 Oct 2021

HAL is a multi-disciplinary open access archive for the deposit and dissemination of scientific research documents, whether they are published or not. The documents may come from teaching and research institutions in France or abroad, or from public or private research centers.

L'archive ouverte pluridisciplinaire **HAL**, est destinée au dépôt et à la diffusion de documents scientifiques de niveau recherche, publiés ou non, émanant des établissements d'enseignement et de recherche français ou étrangers, des laboratoires publics ou privés.



Distributed under a Creative Commons Attribution - NonCommercial 4.0 International License

2D numerical contributions for the study of non-cohesive sediment transport beneath tidal bores

Y. Satria Putra, A. Beaudoin, G. Rousseaux, L. Thomas, S. Huberson.

Department of Fluids, Thermal and Combustion Sciences

*Pprime Institute, UPR 3346, CNRS - University of Poitiers - ISAE ENSMA, TSA 51124,
86073 Poitiers Cedex 9, France.*

Email address: anthony.beaudoin@univ-poitiers.fr

Abstract

2D numerical simulations of tidal bores were obtained using the OpenFOAM CFD software to solve the Navier-Stokes equations by means of the Finite Volume Method by applying a LES turbulence model. The trajectories of non-cohesive sediment particles beneath tidal bores were estimated using a tracker method. Using the fourth order Runge-Kutta scheme, the tracker method solves the Maxey and Riley equations that requires the knowledge of the velocity field at time t . From 2D numerical simulations of tidal bores, we proposed a classification of tidal bores with respect to the Froude number Fr (or r the ratio of water depths). For a Froude number $1 < Fr < 1.43$ ($1 < r < 1.57$), the tidal bore is undular. For a Froude number $1.43 < Fr < 1.57$ ($1.57 < r < 1.75$), the tidal bore is partially breaking, that is similar to the transitional tidal bore defined by Furgerot (2014). And for a Froude number $Fr > 1.57$ ($r > 1.75$), the tidal bore is totally breaking. The numerical results of trajectories of non-cohesive sediment particles are similar to the type of trajectories given by the analytical model proposed by Chen *et al.* (2012) with some modifications to take into account the effects of gravity, elevation and attenuation. The parameters of modified Chen's model, β_1 , β_2 and β_3 , are linearly proportional to the Froude number Fr . This is because the level of turbulence for undular tidal bores is low. The flow induced by an undular tidal bore is not complex. This physical phenomenon is quasi linear. The parameter β_1 , related to the front celerity of the undular tidal bore, decreases when the Froude number Fr increases. The parameter β_2 , related to the elevation, increases when the Froude number Fr increases. And the parameter β_3 , related to the attenuation of the secondary waves, increases when the Froude number Fr increases.

Keywords: Sediment transport, Maxey-Riley equations, tracker method, tidal bore, Froude number, Ratio of water depths, OpenFoam

1. Introduction

The tidal bore is unique phenomenon in the estuaries having a convergent river mouth with a uterine section shape (Fig.1 (a) and (b)). This phenomenon has an influence on the transport of sediment particles in the estuaries as studied by Donnelly and Chanson (2005) in [1]. They observed that the high bed shear stresses induce erosion beneath a tidal bore. There is a lot of studies in the scientific literature that discussed this phenomenon. In field studies, the tidal bore phenomenon has been studied recently by Chanson (2011), Furgerot *et al.* (2016) and Bonneton *et al.* (2016) [2, 3, 4]. In these studies, they have characterized the tidal bore with respect to the Froude number Fr from the field data. Analytically, the tidal bore phenomenon has been studied by Lemoine (1948), Andersen (1978) and Berry (2018) [5, 6, 7]. An analytical study of conjugate depth ratio $r = h_2/h_1$, wavelength L_w and wave amplitude a_w has been presented in these three studies. In the laboratories, the tidal bore phenomenon has been studied by Favre (1935), Treske (1994), Hornung *et al.* (1995), Koch and Chanson (2008) and Rousseaux *et al.* (2016) [8, 9, 10, 11, 12]. In these

studies, two types of tidal bores, undular and breaking, have been generated. The analysis of free surface, velocity and pressure of tidal bores has been performed. And numerically, the tidal bore phenomenon has been studied by Khezri (2013), Simon (2013) and Berchet *et al.* (2018) [13, 14, 15]. They have generated numerical simulations of tidal bores using the CFD software Thétis developed in the I2M laboratory of Bordeaux University, France. This Thétis software has been developed by applying the LES turbulence model to solve the Navier-Stokes equations [13, 14, 15]. The flow pattern of velocity beneath a tidal bore classified into 4 types (*A*, *B*, *C* and *D*) has been performed in the study by Berchet *et al.* (2018).



Figure 1: (a) *Bono* on Kampar river, Indonesia (photograph by Lawrence in [16]) and (b) Kampar river map in Sumatera, Indonesia where the tidal bore *bono* appears (<https://maps.google.com/>).

There is a similitude between a hydraulic jump and a tidal bore. These two phenomena can be characterized by the Froude number Fr , a dimensionless number representing the ratio between the flow inertia to the external field as gravity (see in detail the part 2.1.4). A hydraulic jump is a transition from a supercritical flow with a Froude number $Fr < 1$ to a subcritical flow with a Froude number $Fr > 1$. The tidal bore is also called (improperly) a moving hydraulic jump or a hydraulic bore [2, 17]. The tidal bore is similar to a hydraulic jump because it is generated by the opposite flow of the tide with respect to the river flow. The criteria to generate the tidal bore in nature are well-known: a large tidal range, a shallow and convergent channel, and a low freshwater discharge [18, 4].

To study the impact of tidal bores on the hydrodynamics of river flows, we have referred to some studies of the scientific literature that are correlated with our study. The latter were realized to define the transition between no tidal bore and the undular tidal bore, and the transition between the undular and breaking tidal bores. In their studies, Khezri (2013) and Simon (2013) in [13, 14] generated experimentally and numerically two types of tidal bores, undular and breaking. They used the CFD software Thétis to generate the 2D numerical simulations of tidal bores by applying the LES turbulence model. They have also estimated the wave amplitude a_w and the wavelength L_w from the form of free surface. From their numerical results, the wavelength L_w decreases when the Froude number Fr increases. The wave amplitude a_w increases when the Froude number Fr increases in the regime of undular tidal bore. Otherwise, the wave amplitude a_w decreases when the Froude number Fr increases in the regime of breaking tidal bore. In our study, the numerical study of two tidal bores types, undular and breaking, was done using OpenFOAM (Open Source Field Operation And Manipulation) CFD software by applying a LES turbulence model to complete the studies by Khezri (2013) and Simon (2013). Seventeen 2D numerical simulations were generated to identify the transition from undular tidal bores to breaking tidal bores. A study has been done by Furgerot (2014) in [17] that classified the tidal bores with the Froude number Fr only (not

based on r). She has performed a classification of tidal bores based on the field data where a small wave appears on the tidal bore with a Froude number $Fr < 1.25$. She has also observed that the undular and breaking tidal bores appear with a Froude number $1.25 < Fr < 1.50$ and $Fr > 1.50$ respectively. The low Froude number ($Fr < 1.52$) brings up a low turbulence in the river flow. Then it generates an undular tidal bore in the river channel. For a Froude number $Fr > 1.50$, the high turbulence induces a breaking tidal bore. This classification by Furgerot (2014) in [17] is confirmed and refined in this work using the 2D numerical simulations obtained with OpenFOAM.

To study the impact of tidal bores on the transport of non-cohesive sediment particles, the studies by Chen *et al.* (2012) and Berchet (2014) have been referred in our study [19, 20]. Chen *et al.* (2012) in [19] have studied analytically the trajectory of non-cohesive particles in a two dimensional wave-current field using the fully Lagrangian framework. They have derived analytical solutions that can be used to describe the trajectory of non-cohesive sediment particles beneath an undular tidal bore. Berchet (2014) in [20] has developed a tracker model based on the Maxey-Riley equations to estimate the trajectory of non-cohesive sediment particles under an undular tidal bore. From 2D numerical simulations of undular tidal bores using the CFD software Thétis, he has obtained that the numerical trajectories are similar to those given by the analytical model proposed by Chen *et al.* (2012) in [19]. In our study, we complete the studies by Chen *et al.* (2012) and Berchet (2014) taking into account the effects of gravity, elevation and attenuation on the trajectory of non cohesive sediment particles. Three parameters of the modified Chen’s model, β_1 , β_2 and β_3 , are identified as functions of the Froude number Fr .

In order to reach the two objectives of our study, the study of the impact of tidal bores on the hydrodynamics of river flows and the transport of non cohesive sediment particles, a methodology based on different tools is proposed in the section 2. For the analysis of tidal bore flows, we perform a comparison between the numerical simulations obtained with OpenFOAM [21] and the theory proposed by Lemoine (1948), Andersen (1978) and Berry (2018) [5, 6, 7] for various values of the Froude number Fr , and the ratio of water depths r for Berry only. For the analysis of trajectories of non-cohesive sediment particles, we performe a comparison between the numerical results obtained with a tracker model based on the modified Maxey and Riley equations [22] and the modified Chen’s model [20]. The results of these two comparisons are given in section 3. A validation of 2D numerical simulations obtained with OpenFOAM and a classification of tidal bores are presented in this section. The relationships between the three parameters β_1 , β_2 and β_3 of the modified Chen’s model and the Froude number Fr are given in section 3.

2. Methodology

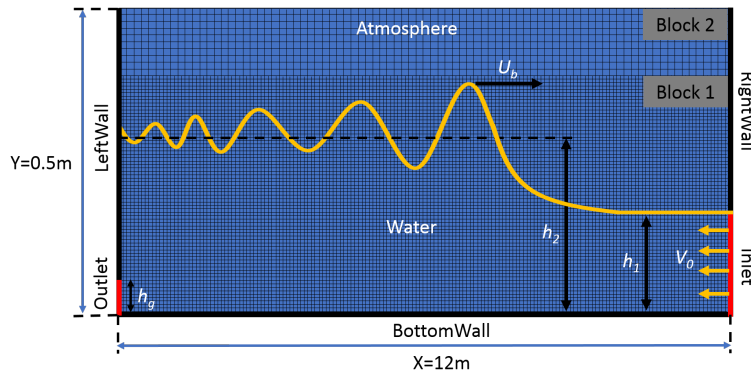


Figure 2: Sketch of computational domain used for the 2D numerical simulations of tidal bores.

In our study, 2D numerical simulations of tidal bores were generated using OpenFOAM (Open Source Field Operation And Manipulation) CFD software. OpenFOAM is an open source CFD software released and developed primarily by OpenCFD Ltd since 2004 [23]. This software uses the Finite Volume discretization and free surface capturing technique based on the Volume of Fluid (VoF) method to solve the Navier-Stokes equations [21]. We have used the LES turbulence model of OpenFOAM, as it has been done by Khezri (2013) and Simon (2013), to generate seventeen 2D numerical simulations of tidal bore. These numerical simulations cover two types of tidal bore, undular and breaking tidal bores. In the LES model, we have used the Smagorinsky model as the turbulence model with a turbulent kinetic energy $k = 0.0001 \text{ m}^2/\text{s}^2$. The viscosity of air and water is set to $\mu_{air} = 1.85 \times 10^{-5} \text{ kg/ms}$ and $\mu_{water} = 10^{-3} \text{ kg/ms}$ respectively. The densities of air and water are set to $\rho_{air} = 1.1768 \text{ kg/m}^3$ and $\rho_{water} = 1000 \text{ kg/m}^3$ respectively, under a gravity acceleration equal to $g = 9.80 \text{ m/s}^2$. The numerical results have been compared with experimental and numerical results by Simon (2013) [14] for undular tidal bores and Khezri (2013) for breaking tidal bores [13].

The 2D computational domain of tidal bores is derived from the experimental setup in an open channel given in Figure 2. The transition between the undular and breaking tidal bores is studied by using the configurations performed by Khezri (2013) [13]. To obtain seventeen 2D numerical simulations of tidal bore that vary in the value of the Froude number Fr , we have set the different gate height h_g for each simulation, between 0 and 0.135 m. The initial flow velocity V_0 and the initial water depth h_1 were fixed to 0.74 m/s and 0.14 m respectively. In these configurations, the size of the 2D computational domain is fixed to 10 m for the length and 0.5 m for the height. The mesh grid of computational domain is generated by the mesh generation utility, *blockMesh* of OpenFOAM. The geometry of computational domain given in Figure 2 was built from a dictionary file, named *blockMeshDict*, located in the *system* directory of OpenFOAM. In the *blockMeshDict* file, we could set the cell number of computational domain Cn . In Figure 2, we divided the computational domain into two blocks. The block 1 is water zone and the block 2 is air zone. The cell number of computational domain could be increased in the block 1 (water zone) and reduced in the block 2 (air zone). The cell number in the block 1 is smoother than the block 2 because in the block 1, the parameters of velocity, pressure and free surface of tidal bore will be calculated. The time step of numerical simulations δt was set in a dictionary file, named *controlDict*, located in the *system* directory of OpenFOAM. These two numerical parameters, cell number of computational domain Cn and time step of numerical simulations δt , will be fixed by a parameter study in subsection 3.1.

2.1. Flow model

2.1.1. Navier-Stokes equations

The flow model of tidal bores is governed by the Navier-Stokes (NS) equations expressed in a velocity-pressure formulation as given in equations 1 and 2:

$$\nabla \cdot (\rho u) = 0, \quad (1)$$

$$\frac{\partial \rho u}{\partial t} + \nabla \cdot (\rho u \phi) - \nabla \cdot (\mu_{eff} \nabla (\rho u)) = -\nabla + \rho g + F_s \quad (2)$$

where u , P , ρ , ϕ and g are the flow velocity (m/s), the pressure (Pa), the fluid density (kg/m³), the flux field of fluid and the gravity acceleration (m/s²) respectively. $\mu_{eff} = \mu + \mu_t$ is the effective dynamic viscosity (kg/m.s) where μ is the kinematic viscosity and μ_t is the turbulent viscosity. F_s (N/m) is the source of momentum which corresponds to the surface tension σ that will be described in the following section. The density ρ in the equation 2 is the density of water and air. The dynamic viscosity and density of fluids, μ and ρ , can be defined as:

$$\mu = \alpha \mu_{water} + (1 - \alpha) \mu_{air}, \quad (3)$$

$$\rho = \alpha \rho_{water} + (1 - \alpha) \rho_{air} \quad (4)$$

where α is the volume fraction of fluid. To express the transport of α was formulated by Weller (2002) in [24] by introducing an extra term in the phase fraction function. It is called the artificial compression term:

$$\frac{\partial \alpha}{\partial t} + \nabla \cdot (\alpha \bar{u}) + \underbrace{\nabla \cdot [u_{\Gamma} \alpha (1 - \alpha)]}_{\text{artificial compression term}} = 0 \quad (5)$$

where u_{Γ} is the vector of the relative velocity between water and air, also called the compression velocity. \bar{u} is the mean velocity calculated by a weighted average of water and air velocities (u_w and u_a):

$$\bar{u} = \alpha u_w + (1 - \alpha) u_a. \quad (6)$$

The Finite Volume method is used to discretize the Navier-Stokes equations [21]. The pressure P is estimated at the cells vertices. The components of the flow velocity u are obtained on the cells sides. The Navier-Stokes equations are integrated on each control volume and discretised in terms of physical fluxes through the control volume faces.

In OpenFOAM, the Volume Of Fluid (VOF) method by Hirt and Nichols (1981) is applied [25]. It uses the volume fraction α as an indicator function (in OpenFOAM called *alpha*) to define the portion of the cell occupied by water. It is defined as:

$$\begin{cases} \alpha(x, y, z, t) = 1 & \text{for a position (x,y,z) occupied by water at a time } t, \\ 0 < \alpha(x, y, z, t) < 1 & \text{for a position (x,y,z) in the interface at a time } t, \\ \alpha(x, y, z, t) = 0 & \text{for a position (x,y,z) occupied by air at a time } t. \end{cases} \quad (7)$$

2.1.2. Surface tension force

The numerical simulation of tidal bores is a multiphase problem where a surface tension appears between air and water. This surface tension is taken into account in the NS equations by means of a surface tension force per unit volume F_s (see Eq. 2). Using a volumetric formulation, the volumetric surface tension force is given by [26]:

$$F_s = \sigma \kappa \nabla \alpha \quad (8)$$

where σ and κ are the surface tension (N/m) and the curvature, respectively.

The difficulty in estimating the surface tension force F_s lies in estimating the curvature κ . In the literature, two families of methods are distinguished to estimate κ , direct derivation from the implicit representation of the interface and discrete differential geometry operators applied to an explicit description of the location of interface [26]. In the first family, the Levelset (LS) methods allow for an accurate estimation of the curvature κ . However the LS methods are found to be non conservative [27] [28]. Still in this first family, the VOF methods tend to provide an inaccurate estimation of the curvature. But they are conservative [29]. Heyns *et al.* have implemented in OpenFOAM a method mixed between LS and VOF methods [30]:

$$\kappa = -\nabla n = -\nabla \cdot \left(\frac{\nabla \alpha}{|\nabla \alpha|} \right). \quad (9)$$

This mixed method is similar to the CSFVOF method of Sussman and Puckett [31].

Taking into account the volumetric form of surface tension force (Eq. 8), the final form of NS equations in equations 1 and 2 can be written as:

$$\nabla \cdot (\rho u) = 0, \quad (10)$$

$$\frac{\partial \rho u}{\partial t} + \nabla \cdot (\rho u \phi) - \nabla \cdot (\mu_{eff}(\nabla \rho u)) = -\nabla p^* + \sigma \kappa \nabla \alpha. \quad (11)$$

130 The NS equations could be solved together with the constitutive relations for the dynamic viscosity (Eq. 3) and the density of fluid (Eq. 4) by using the Finite Volume Method [32].

2.1.3. LES turbulence model

Based on previous works of the scientific literature [33, 34, 35, 36], we have taken the LES model to simulate the turbulent flows of two tidal bore types, undular and breaking. The first 2D numerical simulations of tidal bores, using the Large Eddy Simulation (LES) model, have been realized 135 by Furuyama and Chanson (2008 and 2010) [33, 34]. The lack of mesh grid resolution did not allow to simulate the complete flow dynamic of tidal bores. In 2010, Lubin *et al.* showed that in the 2D numerical simulations the turbulent LES model is able to simulate correctly the main features of breaking tidal bores in accordance with the experimental results, as the time evolution of the free surface [35, 36]. However the agreement between numerical and experimental results of velocity 140 profile is only showed at a selective range of vertical elevation beneath the free-surface [13, 14]. In 2018, Leng *et al.* have performed 3D numerical simulations where the numerical boundary layer presents a thickness close to that of experimental results [37].

Instead of time-averaging, the LES model resolves the large scale motions of flows by solving the spatial-filtered NS equations. In this model, the smaller universal scales, the sub-grid scales (SGS), are modeled. The spatial filtered velocity u of LES model is given by:

$$u(x) = \int_{\Omega} u(x', t) G(x, x', \Delta) ds' \quad (12)$$

145 where $G(x, x', \Delta)$ is the spatial filter with Δ as the filter size, and Ω is the entire space. In LES, the spatial filtering controls the large eddies to be resolved and removes the small eddies to be modelled. To achieve this, spatial filters should be able to smooth away the small eddies [38] [32].

The three filter types are defined in OpenFOAM, *i.e.* *tophat* G_1 , *Gaussian* G_2 and *sharp Fourier cut-off* G_3 . They are expressed as:

$$G_1 = \begin{cases} 1/\Delta^3 & \text{if } |x - x'| \leq \Delta/2, \\ 0 & \text{otherwise,} \end{cases} \quad (13)$$

$$G_2 = \left(\frac{6}{\pi \Delta^2} \right)^{3/2} \exp \left(\frac{-6 \|x - x'\|^2}{\Delta^2} \right), \quad (14)$$

$$G_3 = \prod_{i=1}^3 \frac{\sin \left(\frac{\pi}{\Delta} \|x - x'\| \right)}{\pi \|x - x'\|} \quad (15)$$

where $\Delta = (\Delta_1 \Delta_2 \Delta_3)^{1/3}$ with Δ_i being the filter width in the i -th spatial coordinate [38] [32]. The *tophat* G_1 filter (Eq. 13) was used in this work. This is because the *tophat* G_1 filter is applicable for the finite volume implementation of LES [32]. While for the filters of *Gaussian* G_2 (Eq. 14) and *sharp Fourier cut-off* G_3 (Eq. 15) are implemented for the finite difference implementation of LES. Thus, the spatial filtering defines a new term, the SGS stress tensor τ_{ij}^S . Then, the fluctuation velocity could be expressed as:

$$\overline{u_i u_j} = \overline{u_i u_j} + \overline{u_i' u_j'} = \overline{u_i u_j} - \tau_{ij}^S. \quad (16)$$

Furthermore, the spatially-filtered NS equations is written as:

$$\frac{\partial \bar{u}_i}{\partial t} + \bar{u}_j \frac{\partial \bar{u}_i}{\partial x_j} = -\frac{1}{\rho} \frac{\partial \bar{p}}{\partial x_i} + \frac{1}{\rho} \frac{\partial \bar{\tau}_{ij}}{\partial x_j} - \frac{\partial \tau_{ij}^S}{\partial x_j}. \quad (17)$$

150 2.1.4. Froude number

The strength and free surface shape of tidal bores are linked to the Froude number Fr [39]. Originally, for a channel with an irregular cross-sectional shape and a river flow condition, the Froude number Fr is usually defined as [39]:

$$Fr = \frac{v_0}{\sqrt{g(A/B)}} \quad (18)$$

where v_0 is a river flow velocity (m/s), A is the cross-sectional area (m^2) and B is the free-surface width (m). For open channel flows, the ratio A/B in equation 18 is relevant with the water depth of river h_1 [39]. So, for a rectangular channel, the Froude number Fr is defined as:

$$Fr = \frac{v_0}{\sqrt{gh_1}}. \quad (19)$$

For the tidal bores where the flow velocities of river and tidal bore have opposite directions, the definition of Froude number Fr in equation 19 is written as:

$$Fr = \frac{v_0 + U_b}{\sqrt{gh_1}} \quad (20)$$

with U_b is the front velocity of tidal bore (m/s).

2.1.5. Lemoine's, Andersen's and Berry's theories

In our study, the analysis of tidal bore flows is assessed with theories developed by Lemoine (1948), Andersen (1978) and Berry (2018) [5, 6, 7]. These theories are based on approximations of linear wave theory. Lemoine (1948), Andersen (1978) and Berry (2018) proposed formulas giving the wavelength L_w (m) and the wave amplitude a_w (m) for an undular tidal bore that are expressed in equations 21, 22 and 23 respectively:

$$\frac{L_w}{h_1} = \frac{\pi}{\sqrt{3}}(Fr - 1)^{-1/2} \quad \text{and} \quad \frac{a_w}{h_1} = \frac{8}{3\sqrt{3}}(Fr - 1) \quad (\text{Lemoine's theory}), \quad (21)$$

$$\frac{L_w}{h_1} = \frac{1.79}{(1 - Fr)^{0.614}} \quad \text{and} \quad \frac{a_w}{h_1} = 0.741(Fr - 1)^{1.028} \quad (\text{Andersen's theory}), \quad (22)$$

$$\frac{L_w}{h_1} = 0.3426 \frac{(r + 2)^{3/2}}{\sqrt{(r - 1)}} \quad \text{and} \quad \frac{a_w}{h_1} = 0.2331(r - 1) \quad (\text{Berry's theory}) \quad (23)$$

where $r = h_2/h_1$ is the ratio of water depth of river h_1 (m) to water depth of tidal bore h_2 (m). The ratio r can be written as a function of the Froude number Fr given as [7]:

$$r = \frac{1}{2}(\sqrt{1 + 8Fr^2} - 1). \quad (24)$$

155 Because of this equation, the classification in term of the Froude number is equivalent to the classification in term of r on the assumption of *Bélanger* hypotheses (hydrostaticity, no friction and rectangular geometry). If the friction is included for example, then r will possibly be a function of the Reynolds number Re in addition to the Froude number Fr .

The numerical results of the wave amplitude a_w and wavelength L_w obtained with OpenFOAM are given by the following equations:

$$L_w = X_1 - X_2 \quad \text{and} \quad a_w = \frac{Y_1 - Y_{min}}{2} \quad (25)$$

where Y_{min} (m) is the lowest height between the front and the first stubble (secondary wave), $Y_1(m)$ and X_1 (m) are associated to the front elevation, Y_2 (m) and X_2 (m) are associated to the first stubble elevation. All these quantities are shown in Figure 3.

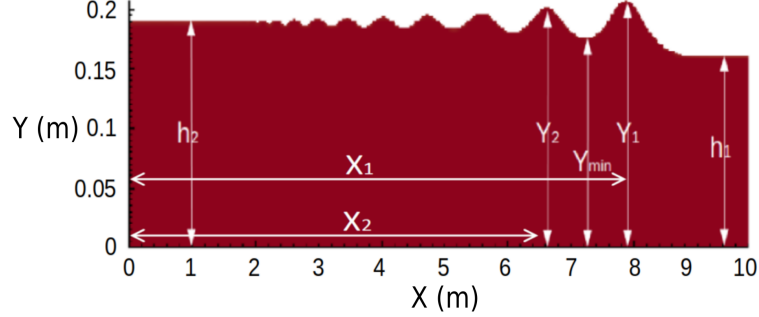


Figure 3: Definition of variables Y_1 , Y_2 , X_1 , X_2 and Y_{min} used in equation 25 to estimate the wave amplitude a_w and the wavelength L_w .

2.2. Transport model

2.2.1. Modified Maxey-Riley equations

A transport model was used to simulate the trajectory of non-cohesive sediment particles. The trajectory of each particle can be described by the fundamental dynamics principle proposed by Maxey and Riley (1983) [22] given in equations 26 and 27:

$$\begin{aligned} \frac{dx_i}{dt} &= v_i(t), \\ m_i \frac{dv_i}{dt} &= V_i (\rho_p - \rho_f) g + m_f \frac{D\vec{u}_i}{Dt} - \frac{1}{2} m_f \frac{d}{dt} \left(v_i - u_i - \frac{1}{10} r_i^2 \nabla^2 u_i \right) \\ &\quad - 6\pi r_i \mu \left(v_i - u_i - \frac{1}{6} r_i^2 \nabla^2 u_i \right) \\ &\quad - 6\pi r_i^2 \mu \int_{t_0}^t \frac{d}{d\tau} \left(v_i(\tau) - u_i(\tau) - \frac{1}{6} r_i^2 \nabla^2 u_i \right) \frac{d\tau}{\sqrt{\pi\nu(t-\tau)}} \end{aligned} \quad (26)$$

where x_i , v_i , m_i , V_i , ρ_i and r_i are the position (m), the velocity (m/s), the mass (kg), the volume (m^3), the density (kg/m^3) and the radius of each particle i respectively at time t (s) to indicates the initial time t_0 (s). Next, m_f , u_i , ρ_f , μ and ν are the mass (kg), the flow velocity (m/s), the density (kg/m^3), the dynamic ($kg/m.s$) and kinematic (m^2/s) viscosity of fluid respectively. The time discretization of the previous system of equations uses the fourth order Runge-Kutta scheme. To obtain the trajectory of non-cohesive sediment particles, it is necessary to have the velocity field during the passage of tidal bores. The flow velocity field is estimated with OpenFOAM.

2.2.2. Modified Chen's model

Chen *et al.* (2012) [19] have computed the particle trajectories in wave-current interaction for a two-dimensional field. In our work, we have proposed three modifications of Chen's model to obtain an analytical solution allowing to analyse the trajectory of non-cohesive sediment particles under undular tidal bores [20, 15]:

- 1 Gravity: Considering a constant settling velocity w_s (m/s), the contribution of gravity in the sediment particle trajectories is given by:

$$y(t) = -w_s(t - t_0). \quad (28)$$

- 2 Elevation: During the passage of an undular tidal bore, an elevation of the free surface appears simultaneously to a slowing down of the river current. Their effects on the sediment particle trajectories can be collected in the same equation with the changing of the water height from h_1 (m) to h_2 (m) and the current velocity from V_1 to V_2 :

$$x(t) = \frac{1}{2\beta_1}((U_1 - U_2) \log(\cosh(-\beta_1)t_B) - \log(\cosh(\beta_1(t - t_B)))) + \beta_1(U_1 + U_2)t, \quad (29)$$

$$y(t) = \frac{h_2 - h_1}{2} \tanh(\beta_2(t - t_B)) \quad (30)$$

180 where t_B is the time taken by the sediment particles to go through the jump front (s), β_1 is the parameter controlling the flow velocity during the slowing down between the two states before and after the front, and β_2 is the parameter controlling the velocity of elevation between the two states.

- 3 Attenuation: The secondary waves (stubbles) amplitude decreases with the distance from the front (see Berry, 2018 [7]). It is probably that the attenuation is a combination of dispersive and dissipative effects to be elucidated. This effect on the sediment particle trajectories can be described by:

$$x(t) = x_{chen}(t) \exp(-\beta_3(t)), \quad (31)$$

$$y(t) = y_{chen}(t) \exp(-\beta_3(t)) \quad (32)$$

185 where β_3 is the attenuation parameter of the related wave-current interaction problem where each stubble is considered as a water wave on its own. x_{chen} and y_{chen} are the coordinates given by the Chen's model [19].

3. Numerical Results

3.1. Convergence study

190 In this convergence study, the undular tidal bore simulation with Froude number $Fr = 1.10$ has been chosen by using the LES turbulence model. The initial velocity and water depth of undular tidal bore were chosen as $V_0 = 0.189$ m/s and $d_0 = 0.2$ m respectively. While for the breaking tidal bore simulation, the initial velocity and water depth are such that $V_0 = 0.74$ m/s and $d_0 = 0.14$ m respectively with Froude number $Fr = 1.48$.

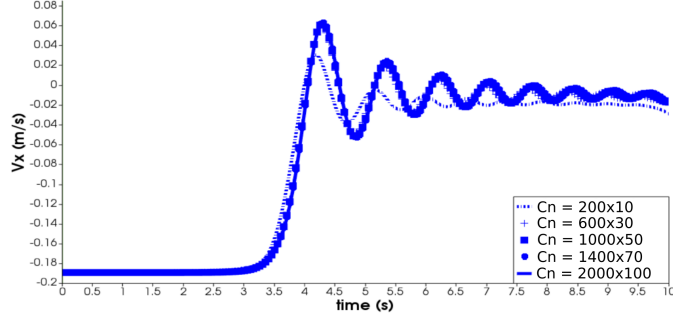


Figure 4: Horizontal component V_x of flow velocity beneath an undular tidal bore with $Fr = 1.10$ at $X = (5 \text{ m}, 0.1 \text{ m})$ using the LES model of OpenFOAM for various values of cell number Cn .

The analysis of cells number Cn of computational domain has been done to generate the tidal bore simulations. The objective is to determine the cells number Cn which provides the best accuracy of numerical simulations. The cells number $Cn = nx \times ny$ has been fixed to 200×10 , 600×30 , 1000×50 , 1400×70 and 2000×100 with nx and ny the discretizations in the two spatial directions. We have observed the time evolution of horizontal component V_x of flow velocity at observation point $X = (5 \text{ m}, 0.1 \text{ m})$ to confirm the convergence of numerical simulations with the cell number Cn in Figure 4. The LES model gives a good convergence for Cn equal to 600×30 , 1000×50 , 1400×70 and 2000×100 . The convergence is reached for $Cn = 600 \times 30$.

3.1.2. Time step δt

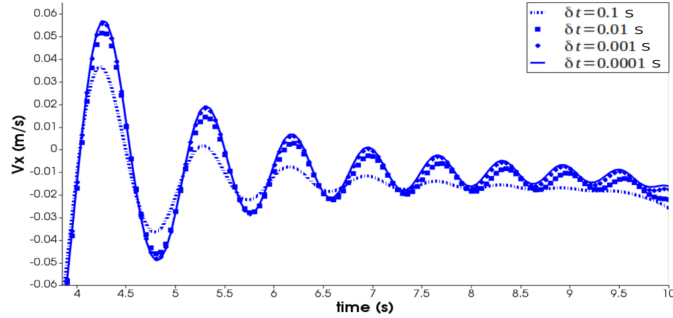


Figure 5: Horizontal component V_x of flow velocity beneath an undular tidal bore with $Fr = 1.10$ at $X = (5 \text{ m}, 0.1 \text{ m})$ using the LES model of OpenFOAM for various values of time step δt .

The convergence study of numerical simulations with the time step $\delta t = 0.1, 0.01, 0.001$ and 0.0001 s has been studied in this section. We have drawn the time evolution of horizontal component V_x of flow velocity at observation point $X = (5 \text{ m}, 0.1 \text{ m})$ in Figure 5. To achieve temporal accuracy and numerical stability, the time step δt must be constrained by the Courant-Friedrichs-Lewy (CFL) condition given by [40]:

$$\delta t_{CFL} = \min \left(\frac{\delta x}{U}, \frac{\delta x^2}{\nu_w} \right) \quad (33)$$

where U is the magnitude of flow velocity and δx is the cell size in the direction x . As the water viscosity ν_w is very small, the first criterion on the advection time imposes the limit of time step δt_{CFL} to ensure the stability of numerical simulations. In our test case, the flow velocity of the

river v_0 being equal to 0.189 m/s , the limit of time step δt_{CFL} is equal to 0.05 s . For the rest of numerical simulations, the time step δt will be fixed to 0.001 s .

210 *3.2. Validation study*

To validate our numerical simulations, we have generated two types of tidal bores, undular and breaking. For the case of undular tidal bores in Figures 6 and 7, the validation of numerical results obtained with OpenFOAM was achieved with analytical, numerical and experimental results obtained in [14, 41] with the Froude number $Fr = 1.10$ compared with the results proposed by Simon (2013) [14]. For the case of a partially breaking tidal bore, the dimensionless time evolution of the free surface, horizontal and vertical components v_x/v_0 and v_y/v_0 of flow velocity have been drawn in Figures 8 and 9 respectively with Froude number $Fr = 1.48$ compared with the results obtained by Khezri (2013) [13].

220 *3.2.1. Undular tidal bore case*

We analyzed the numerical results of the free surface shape for an undular tidal bore at an abscissa $x = 5.15 \text{ m}$ given in Figure 6. At this abscissa, we obtained that the free surface shape has an identical trend with the results of the scientific literature [14, 41]. The wave train generated using OpenFOAM has a similar trend with the numerical results of the free surface using the Thétis code. The free surface shape in Figure 6 shows the similar pattern to the undular tidal bore of type A given by Berchet *et al.* (2018) [15] where the free surface shape is dominated by undulations without global flow reversal but with local flow reversals.

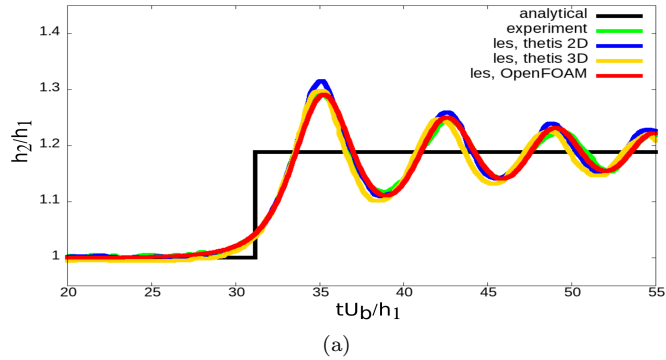


Figure 6: Dimensionless time evolution of the free surface of an undular tidal bore with a Froude number $Fr = 1.10$ at an abscissa $x = 5.15 \text{ m}$ compared with the results proposed by Simon (2013) [14].

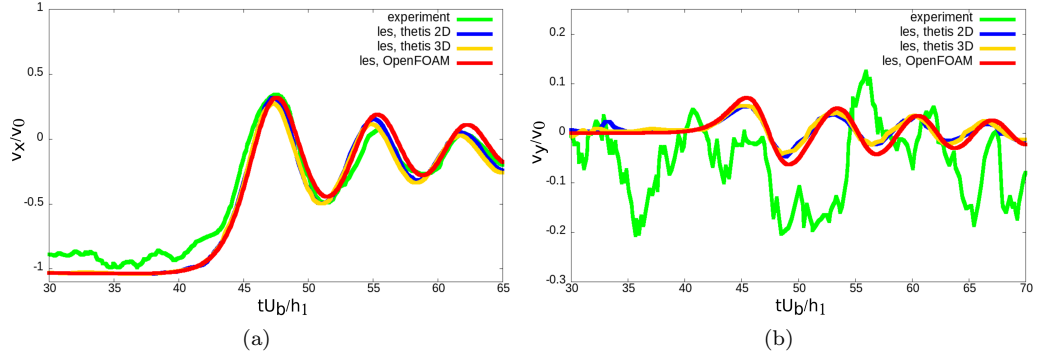


Figure 7: Dimensionless time evolution of the horizontal and vertical components v_x/v_0 (a) and v_y/v_0 (b) of flow velocity for an undular tidal bore with a Froude number $Fr = 1.10$ at a position $X = (7.15 \text{ m}, 0.036 \text{ m})$ compared with the results obtained by Simon (2013) [14].

In Figure 7, we also plotted the dimensionless time evolution of horizontal and vertical components, v_x/v_0 and v_y/v_0 , of flow velocity at a position $X = (7.15 \text{ m}, 0.036 \text{ m})$ for a Froude number $Fr = 1.10$. In this figure, we can observe that the dimensionless time evolution of horizontal and vertical components, v_x/v_0 and v_y/v_0 , of flow velocity obtained with OpenFOAM shows similar trends with the results of the scientific literature in [14, 41]. According to our numerical results in Figure 7, we can observe that the horizontal component v_x/v_0 of flow velocity beneath the crest and trough has positive and negative values respectively. The greatest velocity value occurs beneath the first crest. After that, the velocity value decreases and reaches to the lowest velocity value beneath the first trough. The velocity value re-increases beneath the second crest. However it is smaller than the velocity value beneath the first crest. These numerical results are validated by the numerical and experimental results of the scientific literature [14, 41].

3.2.2. Partially breaking tidal bore case

For the case of breaking tidal bores in Figures 8 and 9, the validation of numerical results obtained with OpenFOAM was achieved with numerical and experimental results obtained in [13]. The numerical results of the free surface shape for a breaking tidal bore have been observed to follow the results obtained by Khezri (2013) at an abscissa $x = 5 \text{ m}$ given in Figure 8. At this abscissa, we obtained that the free surface shape given by OpenFOAM are closer with the results of scientific literature [13].

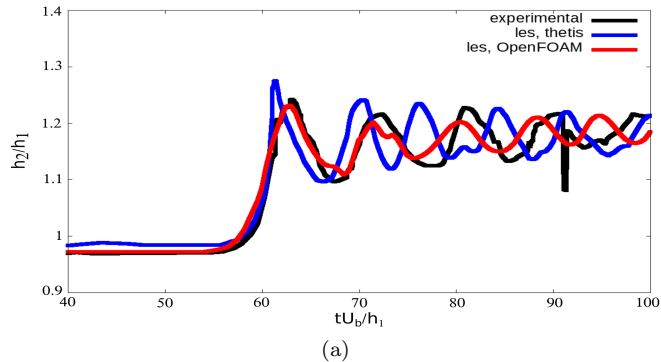


Figure 8: Dimensionless time evolution of the free surface of a partially breaking tidal bore with a Froude number $Fr = 1.48$ at an abscissa $x = 5 \text{ m}$ using OpenFOAM compared with the results reported by Khezri (2013) [13].

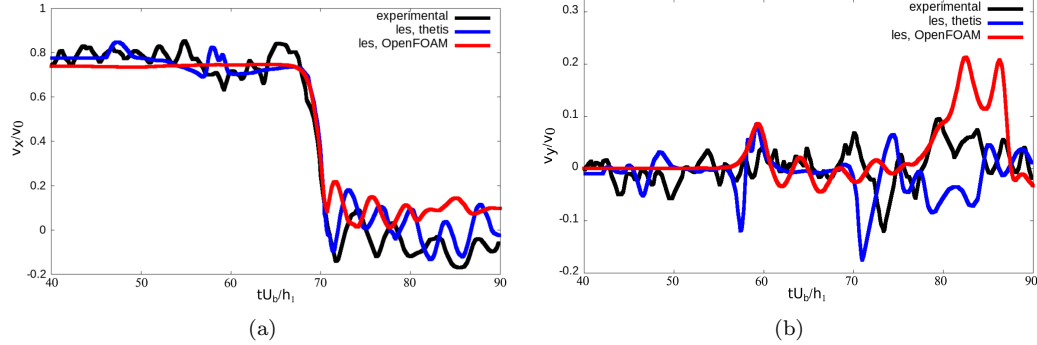


Figure 9: Dimensionless time evolution of the horizontal and vertical components v_x/v_0 and v_y/v_0 of flow velocity for a partially breaking tidal bore with a Froude number $Fr = 1.48$ at a position $X = (5\text{ m}, 0.04\text{ m})$ compared with the results reported by Khezri (2013) [13].

Physically, for a partially breaking tidal bore, the wave amplitude of the front wave is smaller than an undular tidal bore [13]. Based on the experimental photograph by Khezri (2013) in [13], the free surface shape of the front wave for partially a breaking tidal bore is broken and not smooth but still features secondary waves. The free surface shape doesn't have a wave train as in an undular tidal bore. We have also observed that the free surface shape of a partially breaking tidal bore obtained with the OpenFOAM is similar to the numerical results obtained by Lubin *et al.* (2010) in [36].

For a partially breaking tidal bore, the dimensionless horizontal and vertical components, v_x/v_0 and v_y/v_0 , of flow velocity were plotted in Figure 9 at a position $X = (5\text{ m}, 0.04\text{ m})$ (in the water column) by following the work by Khezri (2013) [13] with a Froude number $Fr = 1.48$ using OpenFOAM. According to Figure 9, we can observe that OpenFOAM is close to experimental and numerical given by Khezri (2013). As with experimental and numerical given by Khezri, OpenFOAM produces negative-positive velocity values beneath a partially breaking tidal bore. OpenFOAM gives a numerical simulation similar to the type *C* of Berchet's paper (2018) where the flow velocity is positive $v > 0$ beneath the crest and negative $v < 0$ beneath the trough.

3.3. Classification

Figure 10 shows the dimensionless values of conjugate water depth $r = h_2/h_1$ as a function of the Froude number Fr . In this figure, some reference data are taken from the various papers [8, 42, 9, 43, 44, 14]. Equation 24 as a momentum principle was plotted in this figure. The numerical results of OpenFOAM are in good agreement with the momentum principle and some reference data of the scientific literature. From Figure 10, we confirm that the conjugate depth ratio $r = h_2/h_1$ increases when the Froude number Fr increases.

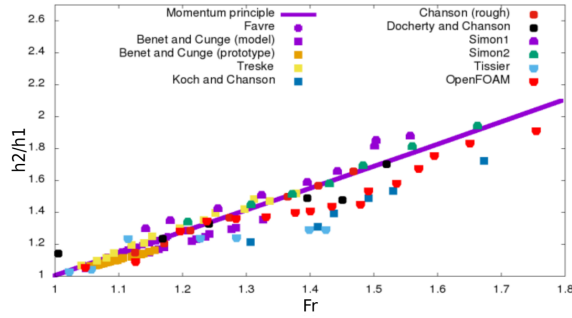


Figure 10: Dimensionless variable h_2/h_1 as a function of the Froude number Fr .

The dimensionless wavelength L_w/h_1 was plotted as a function of the Froude number Fr given in Figure 11 (a). The numerical results of OpenFOAM were compared with the theoretical results given by Lemoine (1948), Andersen (1978) and Berry (2018) in equations 21, 22 and 23 respectively [5, 6, 7]. We also compared the numerical results of OpenFOAM with the experimental results given by Favre (1935), Treske (1994) and Tissier [8, 9, 45]. In Figure 11 (a), we can observe that the numerical results of OpenFOAM follow the trend described in the scientific literature. According to this figure, we obtain that the wavelength L_w decreases when the Froude number Fr increases.

The dimensionless wave amplitude A_w/h_1 was plotted as a function of the Froude number Fr given in Figure 11 (b). The numerical results of OpenFOAM were compared with the theoretical results given by Lemoine (1948), Andersen (1978) and Berry (2018) in equations 21, 22 and 23 respectively [5, 6, 7]. We also compared the numerical results of OpenFOAM with the experimental results given by Favre (1935), Benet and Cunge (1971), Treske (1994), Koch and Chanson (2009), Chanson (2010), Tissier (2011) and Docherty and Chanson (2012) [8, 42, 9, 46, 47, 45, 48]. The numerical results of OpenFOAM were also compared to the field results given by Simpson *at al.* (2004) at Dee river, United Kingdom [49]. The numerical results of OpenFOAM were compared to the numerical results given by Simon (2013) using the Thétis code [14]. According to these comparisons, we obtain that the numerical results of OpenFOAM follow the trend of the scientific literature. We observed that the ratio of wave amplitude a_w/h_1 is even greater when the tidal bore is undular. Then, when the tidal bore turns into a breaking one, the wave amplitude ratio a_w/h_1 of the tidal bore decreases. Figure 11 (b) shows that the transition between a total undular tidal bore and a partial breaking tidal bore is a Froude number $Fr_2 = 1.43$, and the transition between a partial breaking tidal bore and a total breaking tidal bore is a Froude number $Fr_3 = 1.57$. For Froude number $Fr = 1$, the wave amplitude a_w of the tidal bore is difficult to be observed as the free surface of the tidal bore has similarities with the surface of river flow.

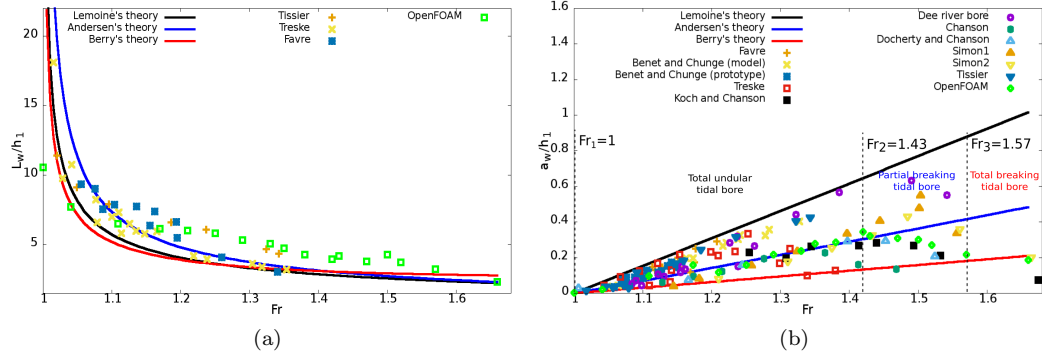


Figure 11: Dimensionless wavelength L_w/h_1 (a) and wave amplitude a_w/h_1 (b) as a function of the Froude number Fr .

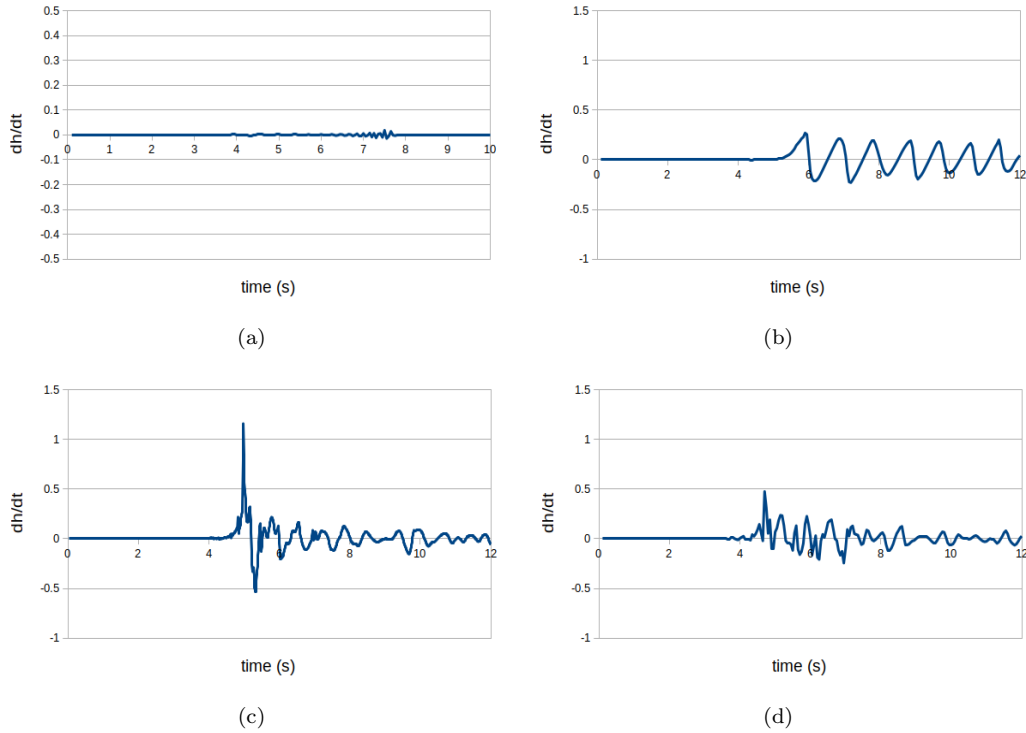


Figure 12: Variation rate of the elevation of free surface dh/dt as a function of time t for the small wave with Froude number $Fr = 1$ (a), the total undular tidal bore with Froude number $Fr = 1.35$ (b), the partial breaking tidal bore with $Fr = 1.43$ (c) and the total breaking tidal bore with $Fr = 1.57$ (d) respectively.

To confirm the values of Fr_1 , Fr_2 and Fr_3 in Figure 11 (b), the variation rate of the elevation of free surface over the time, dh/dt , is studied. In Figure 12, the variation rate dh/dt was drawn for the four conditions of tidal bore: the small wave of tidal bore with the Froude number $Fr = 1$ (Fig. 12 (a)), the total undular tidal bore with Froude number $Fr = 1.35$ (Fig. 12 (b)), the partial breaking tidal bore with $Fr = 1.43$ (Fig. 12 (c)) and the total breaking tidal bore with $Fr = 1.57$ (Fig. 12 (d)). The variation rate dh/dt increases between the Froude number $Fr = 1$ to 1.43 and when the Froude number $Fr = 1.57$, the variation rate dh/dt decreases with the appearance of

strong oscillations. To confirm this analysis, we have referred to the work provided by Furgerot (2014) in [17] that defined the type of tidal bore based on the Froude number Fr . She has observed that for $Fr < 1$ there is no tidal bore, $1 < Fr < 1.5$ is the undular tidal bore, $1.5 < Fr < 1.6$ is the transition of the tidal bore and $Fr > 1.6$ is a breaking tidal bore. Based on the observation of the variation rate of the elevation of free surface dh/dt and Furgerot's classification, we have proposed numerically that for Froude number $1 < Fr < 1.43$ the tidal bore is undular, $1.43 < Fr < 1.57$ the tidal bore is partially breaking that is similar with the tidal bore transition and $Fr > 1.57$ the tidal bore is totally breaking.

3.4. Non-cohesive sediment transport

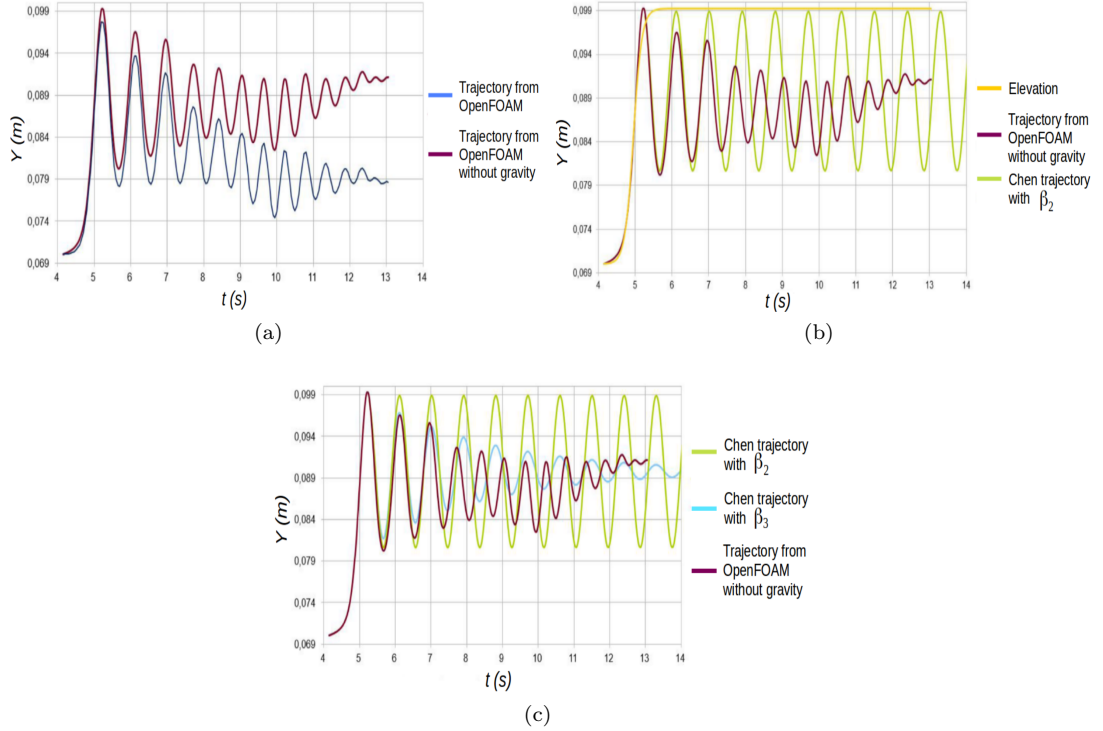


Figure 13: Trajectories of a non-cohesive sediment particle induced by three effects: (a) gravity, (b) elevation and (c) attenuation.

In the case of undular tidal bores, the trajectory of non-cohesive sediment particles were estimated to establish the relationship between the parameters of modified Chen's model, β_1 , β_2 and β_3 , and the Froude number Fr . Figure 13 (a) shows the trajectory of a non-cohesive sediment particle with or without the effect of gravity. By subtracting the contribution of the settling velocity w_s to the complete trajectory, the new trajectory is not affected by gravity. Figure 13 (b) shows the trajectory of a non-cohesive sediment particle obtained with the modified Chen's model considering the effect of elevation. Figure 13 (c) shows the trajectory of a non-cohesive sediment particle obtained with the modified Chen's model considering all the mechanisms, gravity, elevation and attenuation. According to Figure 13, we observe that the three effects of gravity, elevation and attenuation influence the trajectory of non-cohesive sediment particles beneath an undular tidal bore. From Figure 13 (a), we can observe that a trajectory of non-cohesive sediment particles influenced by gravity (blue curve) decreases with increasing the time t . While for the trajectory of non-cohesive sediment particles without gravity (red curve) has a constant value with increasing the time t .

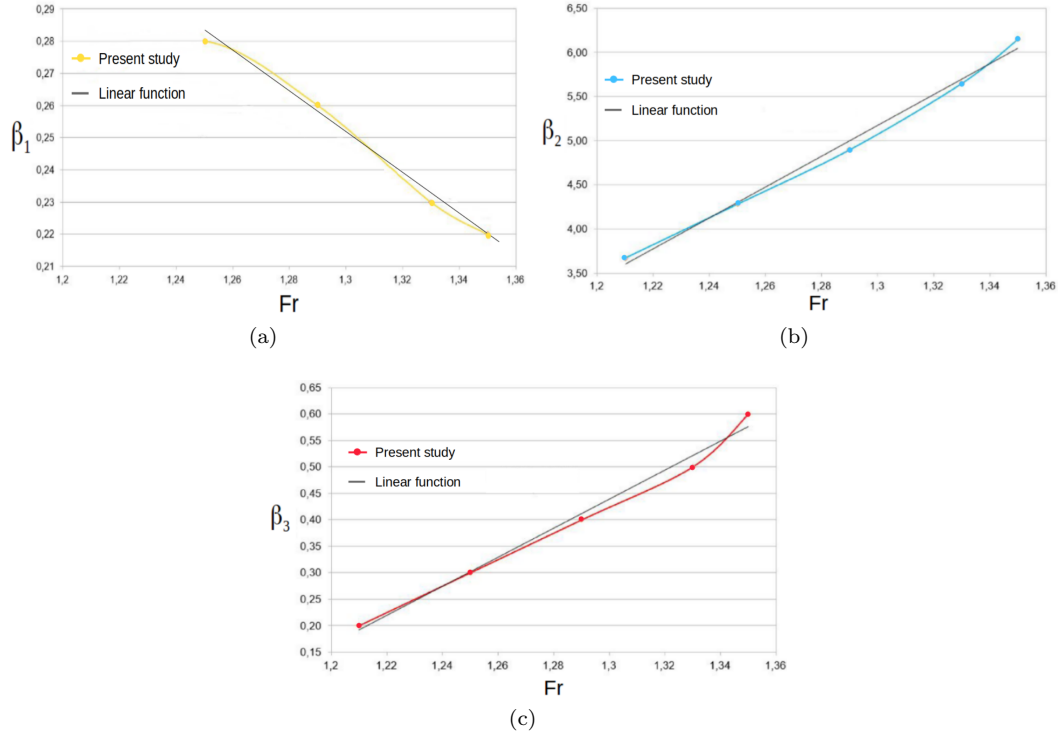


Figure 14: Parameters of modified Chen's model, β_1 (a), β_2 (b) and β_3 (c), as functions of the Froude number Fr in the case of undular tidal bores (the solid line is a fitting linear function).

Figures 14 (a), (b) and (c) show the numerical values of the three parameters of the modified Chens's model, β_1 , β_2 and β_3 , as functions of Froude number Fr . The standard method of least squares was used in order to obtain the best fitting of curves of three parameters, β_1 , β_2 and β_3 :

$$y = -0.41x + 0.78 \quad \text{with} \quad R^2 = 0.98 \quad \text{for} \quad \beta_1, \quad (34)$$

$$y = 17.44x - 17.49 \quad \text{with} \quad R^2 = 0.99 \quad \text{for} \quad \beta_2, \quad (35)$$

$$y = 2.74x - 3.13 \quad \text{with} \quad R^2 = 0.99 \quad \text{for} \quad \beta_3. \quad (36)$$

The least squares fits were plotted in Figures 14 (a), (b) and (c). The relationships between the three parameters, β_1 , β_2 and β_3 , and the Froude number Fr are linear. It may be explained by the low level of turbulence beneath an undular tidal bores. The flow induced by undular tidal bores is not complex. This physical phenomenon is quasi-linear. Thus the theory of wave-current interactions is applicable. Then, the Chen's model can be adapted to the study of undular tidal bores. The parameter β_1 decreases when the Froude number Fr increases (see Fig.14 (a)). The decrease of β_1 means a decrease of the velocity of the tidal bore front. The passage from undular tidal bores to breaking tidal bores induces a slowing of the passage of tidal bores. The two other parameters, β_2 and β_3 , increase with the Froude number Fr (see Fig.14 (b) and (c)). The parameter β_2 simulates the free surface elevation generated by the undular tidal bores passage. The increasing of Froude number Fr induces an increase of this elevation. The flow of tidal bores, being more turbulent, has more energy for producing a more important elevation of free surface. The parameter β_3 simulates the attenuation of the wave train following the tidal bore front. The increase of Froude number Fr induces an increase of this attenuation. The wave train disappears progressively with

340 the Froude number Fr . The breaking tidal bores don't feature this wave train.

4. Conclusions

Using the 2D numerical simulations of tidal bores generated by OpenFOAM, we studied the hydrodynamics of two tidal bores types: undular and breaking. The undular tidal bore type of this study is similar to the tidal bore of type *A* proposed by Berchet *et al.* (2018) [15]. We defined three 345 transitions of tidal bores based on the Froude number Fr . For a Froude number $1 < Fr < 1.43$ ($1 < r < 1.57$), the tidal bore is undular. For a Froude number $1.43 < Fr < 1.57$ ($1.57 < r < 1.75$), the tidal bore is partially breaking, that is similar to the tidal bore transition defined by Furgerot (2014) [17]. And for a Froude number $Fr > 1.57$ ($r > 1.75$), the tidal bore is totally breaking. By using LES turbulence model of OpenFOAM, we have access to the velocity in the water column 350 and the free surface to classify the tidal bore in relation to the free surface and parameterize the modified Chen's model.

The impact of tidal bores on the transport of non-cohesive sediment particles was studied in our work. For the non-cohesive sediment particles, we observed that the trajectory using the flow 355 generated by OpenFOAM is similar to the typical trajectory proposed by Chen *et al.* (2010) [19]. The modifications of Chen's model were done by including the effects of gravity, elevation and attenuation to reproduce non-cohesive particle trajectories under an undular tidal bore. We obtained that the relationships between the parameters of modified Chen's model, β_1 , β_2 and β_3 , and the Froude number Fr are linear. This is because the level of turbulence for undular tidal bores is 360 low. The flow induced by an undular tidal bore is not complex. This physical phenomenon is quasi linear. The parameter β_1 related to the front celerity of tidal bores, decreases when the Froude number Fr increases. We can say that the passage from undular to breaking tidal bores induces a deceleration of tidal bores. The parameter β_2 related to the elevation of tidal bores, increases when the Froude number Fr increases. The tidal bore flow, being more turbulent, has more energy 365 to produce a more important elevation of the free surface. The parameter β_3 , related to the tidal bores attenuation, increases when the Froude number Fr increases. The wave train of undular tidal bores disappears progressively while the Froude number Fr increases. The breaking tidal bores don't present this wave train. The energy associated to this wave train is dissipated by the flow turbulence.

370 As a final remark, we have chosen following the literature to express our results as a function of the Froude number Fr only. For the sake of completeness, we add the range of the r values. Since both parameters are related by the Bélanger equation 24, to choose r or Fr is just a matter of convenience. It seems to us that r is more logical when speaking of the transition to wave breaking 375 instead of the Fr . Bélanger equation should be generalized in order to take into account the potential non-hydrostaticity as well as the structure of the boundary layer as it was done to integrate the effect of the river geometry [39]. Hence, we guess that a future and broader classification of bores taking into account both the free surface (this work) and what happens beneath it (Berchet *et al.*, 2018 [15]), should feature not only the Froude number Fr but others dimensionless numbers 380 like r (encoding wave breaking), the Reynolds number Re (encoding the friction), geometrical parameters like the slope of the banks (encoding curved bore front), etc. This will be our future line of investigation.

5. Acknowledgments

This work is a collaboration between the University of Tanjungpura (Untan), West Kalimantan, 385 Indonesia and the Institute Pprime, University of Poitiers, France with the financing fully covered by the Ministry of Research, Technology and Higher Education of the Republic of Indonesia (Risetdikti). We would like to thank Michael Berry for enlightening discussions on his model.

References

- 390 [1] C. Donnelly, H. Chanson, Environmental impact of undular tidal bores in tropical rivers, *Environmental Fluid Mechanics* 5 (2005) 481–494.
- [2] H. Chanson, *Tidal bores, aegir, eagre, mascaret, pororoqa: theory and observations*, Singapore: World Scientific, 2011.
- 395 [3] L. Furgerot, D. Mouaze, B. Tessier, L. Perez, S. Haquin, Sediment transport induced by tidal bores. an estimation from suspended matter measurements in the see river (mont saint-michel bay, northwestern france), *Comptes Rendus Geoscience* 348 (2016) 432–441.
- [4] P. Bonneton, A. G. Filippini, L. Arpaia, N. Bonneton, M. Ricchiuto, Conditions for tidal bore formation in convergent alluvial estuaries, *Estuarine, Coastal and Shelf Science* 172 (2016) 121–127.
- 400 [5] R. Lemoine, Sur les ondes positives de translation dans les canaux et sur le ressaut ondulé de faible amplitude, *Houille Blanche* (1948) 183–185.
- [6] V. Andersen, Undular hydraulic jump, *Journal of the Hydraulics Division-Asce* 104 (1978) 1185–1188.
- [7] M. Berry, Minimal analytical model for undular tidal bore profile; quantum and hawking effect analogies, *New Journal of Physics* 20 (2018) 1–11.
- 405 [8] H. Favre, *Etude Théorique et Expérimentale des Ondes de Translation dans les Canaux Découverts (Theoretical and Experimental Study of Travelling Surges in Open Channels)*, Publications du Laboratoire de recherches hydrauliques, annexé a l'école polytechnique fédérale de Zurich. Paris: Dunod, 1935.
- 410 [9] A. Treske, Undular bores (favre-waves) in open channels-experimental studies, *Journal of Hydraulic Research* 32 (1994) 355–370.
- [10] H. Hornung, C. Willert, S. Turner, The flow field downstream of a hydraulic jump, *Journal of Fluid Mechanics* 287 (1995) 299–316.
- [11] C. Koch, H. Chanson, Turbulent mixing beneath an undular bore front, *Journal of Coastal Research* 24 (2008) 999–1007.
- 415 [12] G. Rousseaux, J. Mougenot, L. Chatellier, L. David, D. Calluau, A novel method to generate tidal-like bores in the laboratory, *European Journal of Mechanics B/Fluids* 55 (2016) 31–38.
- [13] N. Khezri, Modelling turbulent mixing and sediment process beneath tidal bores: physical and numerical investigations, Ph.D. thesis, School of Civil Engineering, University of Queensland (2013).
- 420 [14] B. Simon, Effects of tidal bores on turbulent mixing : a numerical and physical study in positive surges, Ph.D. thesis, Université de Bordeaux and University of Queensland (2013).
- [15] A. Berchet, B. Simon, A. Beaudoin, P. Lubin, G. Rousseaux, S. Huberson, Flow fields and particle trajectories beneath a tidal bore: A numerical study, *International Journal of Sediment Research*.
- 425 [16] lenstraffic, Bono Tidal Bore Surfing in Sumatera, <http://www.indonesia-tourism.com>, accessible: 4 October 2017.
- [17] L. Furgerot, Propriétés hydrodynamiques du mascaret et de son influence sur la dynamique sédimentaire. une approche couplée en canal et in situ (estuaire de la sée, baie du mont saint-michel), Ph.D. thesis, University of Caen, France (2014).

- 430 [18] S. Bartsch-Winkler, D. K. Lynch, Catalog of worldwide tidal bore occurrences and characteristics, Tech. Rep. Numbered Series Ci no. 1022, USGS (1988).
- [19] Y.-Y. Chen, H.-C. Hsu, H.-H. Wung, Particle trajectories beneath wave-current interaction in a two-dimensional field, *Nonlin. Processes Geophys* 19 (2012) 185–197.
- [20] A. Berchet, Modélisation par des méthodes lagrangiennes du transport sédimentaire induit par les mascarets, Ph.D. thesis, SIMMEA, Université de Poitiers (2014).
- 435 [21] Team, The Open Source CFD Toolbox: Programmer’s Guide, v1706, 28th june 2017 Edition, OpenCFD Limited, 2017.
- [22] M. Maxey, J. Riley, Equation of motion for a small rigid sphere in a nonuniform flow, *Physics of Fluids* 26 (1983) 883–889.
- 440 [23] About OpenFOAM, <https://www.openfoam.com/>, accessible: 13 February 2018.
- [24] H. Weller, Derivation modelling and solution of the conditionally averaged two-phase flow equations, technical report tr/hgw/02 Edition, Nabla Ltd, 2002.
- [25] C. Hirt, B. Nichols, Volume of fluid (vof) method for the dynamics of free boundaries, *Journal of Computational Physics* 39 (1981) 201–225.
- 445 [26] S. Popinet, Numerical models of surface tension, *Annual Review of Fluid Mechancs* 50 (2018) 49–75.
- [27] D. Cassidy, J. Edwards, M. Tian, An investigation of interface-sharpening schemes for multi-phase mixture flows, *Journal of Computational Physics* 228 (2009) 5629–5649.
- [28] Y. Tsui, S. Lin, T. Cheng, T. Wu, Flux-blending schemes for interface capture in two-fluid flows, *International Journal of Heat and Mass Transfer* 52 5547–5556.
- 450 [29] M. Raessi, J. Mostaghimi, M. Bussmann, A volume-of-fluid interfacial flow solver with advected normals, *Computers Fluids* 39 1401–1410.
- [30] J. Heyns, O. Oxtoby, Modelling surface tension dominated multiphase flows using the vof approach, 6th European Conference on Computational Fluid Dynamics.
- 455 [31] M. Sussman, E. Puckett, A coupled level set and volume-of-fluid method for computing 3d and axisymmetric incompressible two-phase flows, *Journal of Computational Physics* 162 (2000) 301–337.
- [32] H. Versteeg, W. Malalasekera, *An Introduction to Computational Fluid Dynamics: the Finite Volume Method*, second edition Edition, Pearson Education Ltd, 2007.
- 460 [33] S.-I. Furuyama, H. Chanson, A numerical study of open channel flow hydrodynamics and turbulence of the tidal bore and dam-break flows, Hydraulic Model Series CH66/08. Australia: School of Civil Engineering, The University of Queensland (2008) p.88.
- [34] S.-I. Furuyama, H. Chanson, A numerical study of a tidal bore flow, *Coastal Engineering Journal* 52.3 (2010) 215–234.
- 465 [35] P. Lubin, S. Glockner, H. Chanson, Numerical simulation of a weak breaking tidal bore, *Mechanics Research Communications* 37 (2010,a) 119–121.
- [36] P. Lubin, H. Chanson, S. Glockner, Large eddy simulation of turbulence generated by a weak breaking tidal bore, *Environmental Fluid Mechanics* 10 (2010,b) 587–602.
- 470 [37] X. Leng, B. Simon, N. Khezri, P. Lubin, H. Chanson, Cfd modeling of tidal bores: development and validation challenges, *Coastal Engineering Journal* (2018) 1–14.

- [38] Y. Gong, F. Tanner, Comparison of rans and les models in the laminar limit for a flow over a backward-facing step using openfoam, in: Nineteenth International Multidimensional Engine Modeling Meeting at the SAE Congress, Detroit, Michigan, 2009.
- 475 [39] H. Chanson, *The Hydraulics of Open Channel Flow: An Introduction*, 2nd Edition, Elsevier Butterworth-Heinemann, 2004.
- [40] X. Xu, X. Deng, An improved weakly compressible sph method for simulating free surface flows of viscous and viscoelastic fluids, *Computer Physics Communications* 201 (2016) 43–62.
- [41] H. Chanson, J. Montes, Characteristics of undular hydraulic jumps: Experimental apparatus and flow patterns, *Journal of Hydraulic Engineering* 121 (1995) 129–144.
- 480 [42] F. Benet, J. A. Cunge, Analysis of experiments on secondary undulations caused by surge waves in trapezoidal channels, *Journal of Hydraulic Research* 9.1 (1971) 11–33.
- [43] C. Koch, H. Chanson, An experimental study of tidal bores and positive surges: hydrodynamics and turbulence of the bore front, Tech. rep., Department of Civil Engineering, University of Queensland (2005).
- 485 [44] H. Chanson, Flow field in a tidal bore: a physical model, Proc. 29th IAHR Congress, Beijing, Theme E, Tsinghua Univers (2001) 365–373.
- [45] M. Tissier, étude numérique de la transformation des vagues en zone littorale, de la zone de levée aux zones de surf et de jet de river., Ph.D. thesis, University of Bordeaux (2011).
- [46] C. Koch, H. Chanson, Turbulence measurements in positive surges and bores, *Journal of Hydraulic Research* 47 (2009) 29–40.
- 490 [47] H. Chanson, Tidal bores, aegir and pororoa: the geophysical wonders, Tech. rep., Congress of IAHR Asia and Pacific Division, IAHR-APD, Auckland, New Zealand (2010).
- [48] N. Docherty, H. Chanson, Physical modeling of unsteady turbulence in breaking tidal bores, *Journal of Hydraulic Engineering* 138 (2012) 412–419.
- 495 [49] J. Simpson, N. Fisher, P. Wiles, Reynolds stress and tke production in an estuary with a tidal bore, *Estuarine, Coastal and Shelf Science* 60 (2004) 619–627.